The Structure of Molecular and Surface Platinum Sites Determined by DNP-SENS and Fast MAS ^{195}Pt Solid-State NMR Spectroscopy

Amrit Venkatesh,[1,2†] Alicia Lund,[3†] Lukas Rochlitz,[4] Ribal Jabbour,[3] Christopher P. Gordon,[4] Georges Menzildjian,[3] Jasmine Viger-Gravel,[5] Pierrick Berruyer, [6] David Gajan,[3] Christophe Copéret,[4] Anne Lesage,[3]* Aaron J. Rossini[1,2]**

[1]*Iowa State University, Department of Chemistry, Ames, IA, USA, 50011.*

[2]*US DOE Ames Laboratory, Ames, Iowa, USA, 50011.*

[3]*Univ Lyon, ENS Lyon, Université Lyon 1, CNRS, High-Field NMR Center of Lyon, FRE 2034, F-69100 VILLEURBANNE, France.*

[4]*Department of Chemistry and Applied Biosciences, ETH Zürich, CH-8093 Zürich, Switzerland.*

[5]*Department of Organic Chemistry, University of Geneva, 1211, Geneva, Switzerland.*

[6]*Institut des Sciences et Ingénierie Chimiques, Ecole Polytechnique Fédérale de Lausanne (EPFL), CH-1015, Lausanne, Switzerland.*

Corresponding Authors

*e-mail: ccoperet@ethz.ch

*e-mail: anne.lesage@ens-lyon.fr

*e-mail: arossini@iastate.edu

Author Contributions

[†]These authors contributed equally.

ABSTRACT

The molecular level characterization of heterogeneous catalysts is challenging due to the low concentration of surface sites and the lack of techniques that can selectively probe the surface of a heterogeneous material. Here, we report the joint application of room temperature proton-detected NMR spectroscopy under fast magic angle spinning (MAS) and Dynamic Nuclear Polarization Surface Enhanced NMR Spectroscopy (DNP-SENS), to obtain the ^{195}Pt solid-state NMR spectra of a prototypical example of highly dispersed Pt sites (single site or single atom), here prepared via Surface Organometallic Chemistry, by grafting [(COD)Pt(OSi(O*t*Bu)$_3$)$_2$] (**1**, COD = 1,5-cyclooctadiene) on partially dehydroxylated silica (**1@SiO$_2$**). Compound **1@SiO$_2$** has a Pt loading of 3.7 wt.%, a surface area of 200 m^2/g, and a surface Pt density of around 0.6 Pt site/nm^2. Fast MAS ^{1}H{^{195}Pt} dipolar-HMQC and S-REDOR experiments were implemented on both the molecular precursor **1** and on the surface complex **1@SiO$_2$**, providing access to ^{195}Pt isotropic shifts and Pt-H distances, respectively. For **1@SiO$_2$**, the measured isotropic shift and width of the shift distribution help constrain the ^{195}Pt chemical shift tensor parameters fitted on the static wideline DNP-enhanced ^{195}Pt spectrum. Overall the NMR data provide evidence for a well-defined, single-site structure of the isolated Pt sites.

Introduction

Heterogeneous catalysis is arguably one of the most influential technologies of modern life owing to its wide utilization in environmental depollution and numerous industrial chemical processes.[1-2] Establishing structure-activity relationships of heterogeneous catalysts poses a considerable challenge, making the rational design and improvement of these typically complex materials difficult. Recently single-site and single-atom catalysts,[3] in which the active phase is highly dispersed, have offered the opportunity to discover new reactivity and to gain molecular-level insight into active site structure and reaction mechanisms. In parallel, Surface OrganoMetallic Chemistry (SOMC)[2, 4-5] has emerged as a powerful tool to generate well-defined surface sites that can be used either directly as single-site catalysts or can be used as precursors to control the growth, composition and interface of supported nanoparticles.[6-9] SOMC relies on the detailed characterization of surface species and has benefited tremendously from advanced solid-state NMR (SSNMR) spectroscopy. SSNMR spectroscopy has predominantly been used to characterize the structure of the ligands attached to the metal centers, although in some favorable cases the metal centers have also been directly probed.[10-17]

Platinum is an important element used in catalysis, finding applications in numerous processes such as alkane dehydrogenation,[18] CO oxidation,[19] the water-gas shift reaction[20] etc. While typically used in the form of nanoparticles, Pt has recently been proposed to also participate in catalytic reactions when dispersed as a single-atom (Figure 1A).[3, 19, 21-22] Such isolated metal sites can readily aggregate and redisperse as a function of reaction conditions to generate the active sites and complex–nanoparticle support interfaces. While isolation of Pt sites may be confirmed by atomically resolved microscopy, understanding the molecular and electronic structure of such isolated sites remains a major challenge in catalysis.

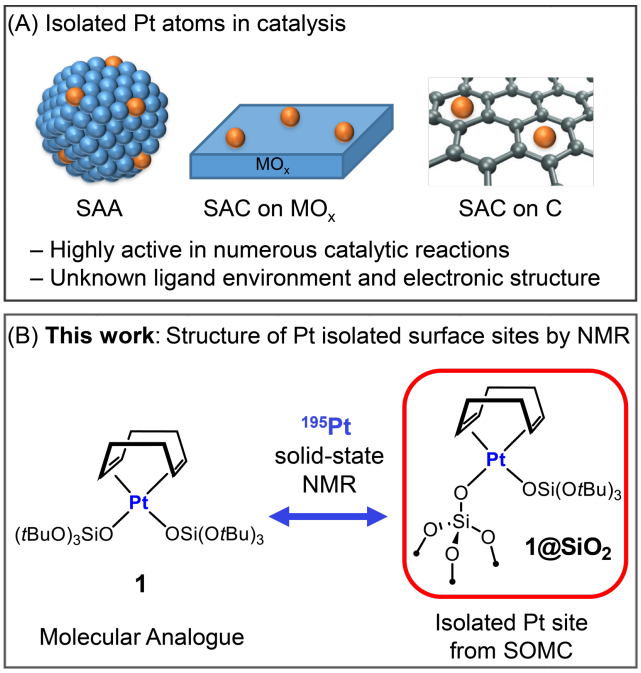

Figure 1. A) Schematic representation of Pt isolated sites used in catalysis in the form of so-called single atom alloy (SAA)[23] and single atom catalysts (SAC) on metal oxides or carbon-based materials.[3, 24-25] (B) Methodology to establish ^{195}Pt SSNMR as a tool to obtain structural information of Pt isolated sites.

^{195}Pt SSNMR can provide valuable information on the local chemical environment and electronic structure of Pt centers because of the reliance of the chemical shift tensor on the identity and symmetry of the surrounding ligands.[26-37] However, the low sensitivity of ^{195}Pt NMR and sparse metal surface sites (< 4 wt.%) make direct characterization of the local environment of Pt metal centers on surfaces by SSNMR challenging. Although ^{195}Pt is a spin-½ nucleus with a moderate Larmor frequency (ν_0 = 85.896 MHz at 9.4 T) and natural abundance of 33%, ^{195}Pt SSNMR spectra are often severely broadened by chemical shift anisotropy (CSA), resulting in poor NMR sensitivity. Schurko and co-workers have reported wideband excitation techniques such as adiabatic inversion cross polarization (BRAIN-CP)[38] and WURST-based Carr-Purcell-Meiboom-Gill echo-train acquisition (WCPMG)[39] that allow static wideline SSNMR spectra to be acquired with improved sensitivity. Dynamic nuclear polarization surface enhanced NMR spectroscopy (DNP-SENS) has recently emerged as a versatile and unique approach to increase

the NMR sensitivity of surface sites in materials science, enabling the implementation of advanced experiments within reasonable experimental times on dilute species.[12, 40-43] BRAIN-CP-WCPMG experiments have been applied in combination with DNP for the acquisition of static wideline ^{195}Pt NMR spectra of Pt^{2+} ions coordinated to MOF linkers.[33] DNP was also used to obtain BRAIN-CP-WCPMG and cross-polarization magic angle spinning (CPMAS) ^{1}H→^{195}Pt SSNMR spectra of an organometallic platinum complex supported on zinc-modified silica.[36]

The sensitivity of conventional SSNMR spectroscopy has also been enhanced dramatically using fast magic angle spinning (MAS) and proton detection techniques in the last two decades.[44] Fast MAS has also been shown to improve sensitivity for SSNMR experiments on heavy spin-1/2 nuclei with large CSA by focusing signal intensity into fewer spinning sidebands.[45] Fast MAS ^{1}H{^{195}Pt} dipolar heteronuclear multiple quantum coherence spectroscopy (D-HMQC) enables the rapid determination of ^{195}Pt isotropic chemical shifts and/or acquisition of spinning sideband manifolds.[35, 46-48] ^{1}H{^{195}Pt} magic angle turning (MAT) D-HMQC was also used to observe coordination of Pt^{2+} ions to MOF linkers.[35] However, D-HMQC solid-state NMR experiments are often hindered by t_1-noise. Recently, we demonstrated t_1-noise eliminated (TONE) D-HMQC pulse sequences that reduce t_1-noise in 2D D-HMQC spectra, paving the way for fast MAS TONE D-HMQC to be used for observation of low-concentration single-atom ^{195}Pt species.

Here, we report the joint application of room temperature fast MAS ^{1}H{^{195}Pt} TONE D-HMQC and S-REDOR SSNMR experiments, and cryogenic DNP-SENS experiments to obtain and interpret ^{195}Pt SSNMR spectra of isolated Pt sites, obtained by grafting the molecular precursor [(COD)Pt(OSi(O*t*Bu)$_3$)$_2$] (**1**, COD = 1,5-cyclooctadiene)[49] on partially dehydroxylated silica at 700°C (**1@SiO$_2$**, Figure 1B). **1@SiO$_2$** is used as a prototypical example of a highly dispersed metal site with 0.6 Pt site/ nm^2, relevant to single-site or single-atom catalysts.[6]

Experimental

Synthesis of materials: All operations were performed in a M. Braun glove box under an argon atmosphere. All solvents were dried using standard procedures. **$SiO_{2\text{-}700}$** was prepared by heating Evonik AEROSIL® (200 m^2/g) to 500 °C (ramp of 300 °C/h) in air and calcined at this temperature for 12 hours. The calcination was followed by evacuation to high vacuum (10^{-5} mbar) while maintaining the temperature at 500 °C for further 8 hours, heating to 700 °C (ramp of 60 °C/h), and maintaining at 700 °C for 24 hours. Titration of the resulting **$SiO_{2\text{-}700}$** using $[Mg(CH_2Ph)_2(THF)_2]$ purified *via* sublimation prior to use, yielded an Si-OH density of 0.3 mmol/g, corresponding to 0.9 accessible Si-OH groups per nm^2. The molecular complex $[Pt(OSi(OtBu)_3)_2(COD)]$ (**1**) was prepared according to a literature procedure.[49]

$[Pt(OSi(OtBu)_3)_2(COD)]/SiO_2$ (1@SiO_2) was prepared according to an adapted literature procedure.[6] **$SiO_{2\text{-}700}$** (1.465 g, 0.440 mmol -OH) was added to a 100 ml Schlenk flask. Benzene (about 10 ml) was added slowly while stirring to give a white suspension. $[Pt(OSi(OtBu)_3)_2(COD)]$ (0.346 g, 0.420 mmol, 0.285 mmol/OH) was added slowly to the suspension as a colorless solution in benzene (about 10 ml) while stirring (100 rpm). The resulting suspension was stirred for 12 h at rt. The benzene on top of the silica material was decanted and the material washed with benzene (10 ml) three times to wash off unreacted complex. The material was then washed with pentane before it was dried under high vacuum (10^{-5} mbar) for 4 h to remove residual solvent yielding **$[Pt(OSi(OtBu)_3)_2(COD)]/SiO_2$** as a white solid (**1@SiO_2**). Elemental analysis showed 3.73 wt% Pt, 4.76 wt% C and 0.79 wt% H, which are in good agreement with one COD and one siloxide ligand per Pt atom on the surface.

Fast MAS ^{1}H-^{195}Pt experiments: Experiments were performed at 9.4 T using a Bruker 1.3 mm double resonance probe, Bruker Avance III HD spectrometer and a Bruker wide-bore NMR magnet. Rotors were packed in the glovebox and spun using N_2 gas for NMR experiments. ^{1}H and ^{195}Pt chemical shifts were referenced indirectly to neat tetramethylsilane by using the ^{1}H shift of adamantane (1.82 ppm) as a secondary standard. All fast MAS $^{1}H\{^{195}Pt\}$ experiments were performed using $SR4_1^2$ heteronuclear dipolar recoupling.[50] Prior to quantitative 1D experiments and 2D experiments, ^{1}H longitudinal relaxation time constants (T_1) were measured with a saturation recovery spin echo pulse sequence. The States-TPPI procedure[51] was used for 2D spectral acquisition unless mentioned otherwise. ^{1}H 90° and 180° pulses of 2.5 and 5 μs duration was used in all experiments. ^{195}Pt SHAPs used tanh/tan shapes with a 20 μs duration, *ca.* 275 kHz rf and 5 MHz sweep width. 0.6 μs pulses at *ca.* 275 kHz rf were used for ^{195}Pt excitation in the HMQC experiments.[46] Analytical simulations were performed either with the TopSpin solid lineshape analysis module (sola) or ssNake *v*1.1.[52]

^{1}H spin echo spectra were collected with a 3.5 s recycle delay that was equal to 5 × T_1. All subsequent experiments on **1** were performed with a 0.91 s recycle delay equal to 1.3 × T_1. ^{1}H spin echo spectra and $^{1}H\{^{195}Pt\}$ TONE D-HMQC-4 spectra shown in Figure 2B were obtained with 8 and 64 scans, respectively. The total duration of $SR4_1^2$ recoupling was 1.6 ms at 50 kHz MAS, or 1.57 ms at 51 kHz MAS and was optimized to give optimal signal in a 1D TONE D-HMQC-4 experiment at 50 kHz MAS. 2D rotor-synchronized $^{1}H\{^{195}Pt\}$ TONE D-HMQC-4 spectra on **1** were obtained with 8 scans, 96 t_1 increments with a 50 or 51 F_1 kHz spectral width, depending on the MAS frequency. The total duration of the LG spin-lock pulse was set to 50 rotor cycles and the rf field was 130 kHz. Details regarding the implementation of LG spin-lock pulses at fast MAS was reported previously.[53]

The $^{1}H\{^{195}Pt\}$ TONE D-HMQC-4 spectrum of **1** shown in Figure 4B and Figure S6 was obtained with 80 scans, 3136 t_1 increments and a 1 MHz F_1 spectral width. The States-TPPI procedure was used to achieve sign discrimination in F_1. The total duration of the LG spin-lock pulse was set to 80 rotor cycles and the rf field was 130 kHz.

In case of **1@SiO$_2$**, the sample was cooled down to *ca.* 275 K to avoid any potential degradation. The ^{1}H spin echo spectrum was obtained with a 5.5 s recycle delay ($5 \times T_1$) and all other experiments used an optimal recycle delay of 1.43 s ($1.3 \times T_1$). ^{1}H spin echo spectra and $^{1}H\{^{195}Pt\}$ TONE D-HMQC-4 spectra shown in Figure 2C were obtained with 64 and 600 scans, respectively. 2D $^{1}H\{^{195}Pt\}$ TONE D-HMQC-4 spectra were acquired with 600 scans, a F_1 spectral width equal to the MAS frequency and 40 t_1 increments. The total LG spin-lock pulse duration was set to 50 rotor cycles with an rf field of 130 kHz. The total duration of $SR4_1^2$ recoupling was ca. 1.76 ms at 50 kHz MAS, 1.6 ms (at 55 kHz MAS), and 1.78 ms at 45 kHz MAS). The recoupling duration was optimized to give optimal signal in a 1D TONE D-HMQC-4 experiment at 50 kHz MAS. The conventional D-HMQC spectra shown in Figure S4 were acquired using 600-768 scans and with all other conditions the same as for the TONE D-HMQC-4 experiments.

$^{1}H\{^{195}Pt\}$ S-REDOR experiments[54] were performed with 128 and 352 scans for **1** and **1@SiO$_2$**, respectively. The control (S_0) and dephased (S) experiments were performed in an interleaved fashion. 1-(S/S_0)-ϕ was then plotted as a function of recoupling duration. The term 'ϕ' represents an intensity offset to account for an additional 0th order phase observed in the first dephased (S) spectrum.[55] The ϕ values for **1** and **1@SiO$_2$** were set to 0.08 and 0.05, respectively based upon the value of 1-(S/S_0) measured for the first data point.[55] SIMPSON simulations of the S-REDOR curves were performed with a rep320 crystal file (α, β) and 33 gamma angles for powder averaging. An ideal π pulse was used on the ^{1}H channel and other details including the

^{195}Pt CS tensor and SHAP parameters were included in the simulations. The ^{1}H-^{195}Pt dipolar couplings corresponding to the distances specified in Figures 5 and S9 were varied to obtain the different curves.

*Static ^{195}Pt experiments of **1** at 11.7 T*: Static experiments were performed on compound **1** using a Bruker 4 mm double resonance MAS probe on a 500 MHz wide bore Bruker AVANCE III Bruker NMR spectrometer. The sample was packed into a 4 mm zirconia rotor in a glove box. The ^{195}Pt chemical shift was referenced to an aqueous solution of K_2PtCl_4. The BRAIN-CP-WCPMG pulse sequence (Figure S5, but without microwave irradiation) was performed using the variable offset cumulative spectrum (VOCS) procedure.[56] A ^{1}H excitation pulse of 5 μs was used followed by a 10 ms contact time, with WURST A swept over 400 kHz applied to ^{195}Pt. For detection 50 μs WURST B and C pulse were swept over 500 kHz with a spikelet separation of 5 kHz. A recycle delay of 1.5 s was used and 2048 scans were accumulated. The transmitter offset between sub-spectra was 200 kHz. Analytical simulation of the static ^{195}Pt spectrum was performed using a two-site model on ssNAKE software.[52] The isotropic shifts determined from the MAS experiments was fixed for the two sites (Figure 3A). The span (Ω) of both CS tensors was fixed to 8150 ppm and the skew (κ) was adjusted to -0.73 to yield the best fit.

*Static DNP-SENS ^{195}Pt experiments of **1@SiO$_2$** at 9.4 T*: The static DNP SENS experiments were performed using a Bruker AVANCE III wide bore 400 MHz/263 GHz DNP spectrometer.[57] The ^{195}Pt chemical shift was referenced to an aqueous solution of K_2PtCl_4. The DNP sample of compound **1@SiO$_2$** was prepared in a glove box and impregnated with a solution of 16 mM TEKPol[58] radical in 1,1,2,2-tetrachloroethane (TCE) via the incipient wetness method and packed into a 3.2 mm sapphire rotor. The DNP sample was immediately inserted into a Bruker 3.2 mm low-temperature MAS DNP probe precooled to 100 K. The static DNP ^{195}Pt spectra were acquired

using the BRAIN-CP-WCPMG pulse sequence[38] with microwave irradiation as shown Figure S5. Continuous microwave irradiation was generated by a gyrotron operating at a frequency of 263 GHz and with an approximate power of 40 W. A ^{1}H excitation pulse of 2.5 us was used followed by a 10 ms contact time, with WURST A swept over 400 kHz applied to ^{195}Pt. For detection 50 μs WURST B and C pulse were swept over 500 kHz with a spikelet separation of 5 kHz. A recycle delay of 7 s was used and 4096 scans were accumulated. Variable offset accumulation was used, and seven different offset frequencies were acquired by stepping the transmitter by 100 kHz.

The lineshape fitting was carried out using the software package DMFIT[59] using a static CSA model parametrized in the Herzfeld-Berger convention. The isotropic chemical shift was fixed to the values determined with MAS TONE D-HMQC experiments under fast MAS and the other parameters were optimized. A Gaussian line broadening of ca. 8 kHz was necessary to obtain a satisfying fit, in good agreement with the data presented on Figure 3B.

*MAS DNP-SENS ^{13}C and ^{29}Si experiments of **1@SiO$_2$** at 9.4 T*: In addition to the static ^{195}Pt experiment, MAS experiments with the DNP sample of compound **1@SiO$_2$** were performed at 8 kHz MAS and 100 K. The DNP-SENS ^{1}H→^{13}C cross-polarization magic angle spinning (CPMAS) spectrum of **1@SiO$_2$** was acquired using the solvent suppression sequences developed by Yarava *et al* (Figure S7).[60] The DNP-SENS ^{1}H→^{29}Si CPMAS spectrum of **1@SiO$_2$** was also acquired and found to have an enhancement of 80 (Figure S8).

Molecular DFT calculations: Molecular structures were optimized with the Gaussian09 package[61] using the PBE0 functional.[62] Pt was represented by the fully-relativistic effective core potential (RECP) from the Stuttgart group and the associated basis sets.[63] The remaining atoms (H, C, O, Si) were represented by a triple-ζ cc-pVTZ basis set.[64] NMR calculations were performed using ADF 2014[65] with the PBE0 functional and Slater-type basis sets of quadruple-ζ quality

(QZ4P) for Pt and triple-ζ quality (TZP) for other atoms. Relativistic effects were treated by the 2 component zeroth order regular approximation (ZORA).[66] The 3D representation of the calculated shielding tensors were obtained as polar plots[67] of functions $\sum_{ij} r_i \sigma_{ij} r_j$. The calculated ^{195}Pt chemical shifts were referenced to (COD)$PtCl_2$, with an experimental isotropic chemical shift of -3360 ppm, and a calculated isotropic shielding of 5483 ppm.

Plane-wave DFT calculations: Optimization of the hydrogen atom positions of **1** using plane-wave DFT with the previously reported crystal structure.[49] The CASTEP[68] program was used with the PBE-GGA functional[69], TS dispersion correction scheme[70] and ultra-soft pseudopotentials.[71] The GIPAW method[72] with the Zero-Order Relativistic Approximation (ZORA)[73] was used to calculate the magnetic shielding tensors. A *k*-point spacing of 0.07 $Å^{-1}$ was used for the Monkhorst-Pack grid.

Results and Discussion

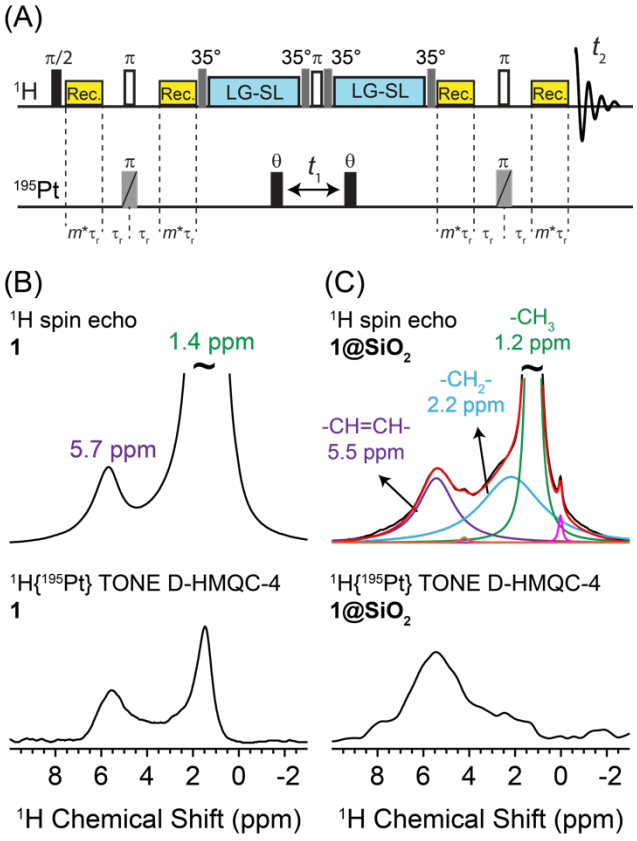

Figure 2. (A) TONE D-HMQC-4 pulse sequence used to perform 1D and 2D ^{1}H{^{195}Pt} D-HMQC experiments, (B) (top to bottom) 1D ^{1}H spin echo and 1D ^{1}H{^{195}Pt} TONE D-HMQC-4 of **1** and **1@SiO$_2$**. Spectra were acquired with a 50 kHz MAS frequency and B_0 = 9.4 T.

Figure 2A shows the TONE D-HMQC-4 pulse sequence used for acquisition of ^{1}H-detected ^{195}Pt SSNMR spectra. This pulse sequence requires application of two inversion pulses on the ^{195}Pt channel.[74] However, broadband inversion is challenging with rectangular pulses due to the large CSA associated with square-planar Pt compounds and the limited radio frequency (rf) fields available. Short high-powered adiabatic pulses (SHAP)[75-76] were previously used for efficient inversion of ^{195}Pt SSNMR spectra in magic angle turning (MAT) D-HMQC experiments.[35] Therefore, SHAPs were also used in the TONE D-HMQC-4 sequence for broadband inversion. Furthermore, SHAPs are also incorporated into the symmetry-based

resonance-echo double resonance (S-REDOR) pulse sequence[54] to measure ^{1}H-X heteronuclear dipolar couplings and internuclear distances (Figure S1). Further details regarding the implementation of SHAPs in TONE D-HMQC and S-REDOR experiments will be discussed in a separate future publication. Figure 2B and 2C show 1D ^{1}H spin echo and ^{1}H{^{195}Pt} TONE D-HMQC-4 spectra of **1** and **1@SiO$_2$**, respectively. The ^{1}H NMR signals at 1.2-1.4 ppm and 5.5-5.7 ppm are assigned to the methyl protons of the tert-butyl groups and to the olefinic protons in the COD ligand, respectively. The ^{1}H SSNMR spectrum of **1@SiO$_2$** displays higher resolution than **1** due to the reduction in ^{1}H concentration for the surface species. The improved resolution in **1@SiO$_2$** allows observation of the ^{1}H signals at 2.2 ppm from CH_2 protons in the COD ligand (Figure 2C). The integrated signal intensities of the ^{1}H spin echo spectra of **1** and **1@SiO$_2$** are consistent with the structures; the slight reduction in the integrated intensity of the methyl signals in **1@SiO$_2$** is attributed to the difficulty of deconvolving signals with significant overlap (Figure S2). Elemental analysis of **1@SiO$_2$** also confirmed the proposed structure shown in Figure 1B (*vide supra*). The signal at 4.2 ppm is tentatively assigned to an OH group corresponding to a small fraction of hydrogen-bonded silanol[77] or isobutene-related species (Figure S3A). These spectral assignments are in good agreement with the ^{1}H 2D double quantum spectrum (Figure S3B).

Short ^{1}H T_1 of 0.7 and 1.1 s in **1** and **1@SiO$_2$**, respectively, make fast MAS D-HMQC experiments favorable for the indirect detection of ^{195}Pt SSNMR spectra. A 1D ^{1}H{^{195}Pt} TONE D-HMQC-4 spectrum of **1** was acquired in only 1 minute and shows an intense signal from the vinyl protons that are *ca.* 2.6 Å from the Pt metal center (Figure 2B, bottom spectrum). Despite the lowered ^{195}Pt concentration in **1@SiO$_2$** (< 4 wt.% Pt) a 1D ^{1}H{^{195}Pt} TONE D-HMQC-4 spectrum was obtained in only 14 minutes (Figure 2C, bottom spectrum). This result illustrates the value of fast MAS, proton-detected methods. The sensitivity of the 1D ^{1}H{^{195}Pt} TONE D-

HMQC-4 spectra, which is defined as the signal-to-noise ratio (SNR) per square root of unit time, is reduced from 28.4 $min^{-1/2}$ for **1** to 2.4 $min^{-1/2}$ for **1@SiO₂**. The factor 12 reduction in sensitivity (28.4/2.4 $min^{-1/2}$) is proportional to the reduction in absolute ^{1}H SSNMR signal intensities and primarily arises because of the decreased Pt loading from **1** to **1@SiO₂** (from *ca.* 23 wt.% to ca. 4 wt.%) and the lower density of silica as compared to microcrystalline **1**. The ca. 12-fold reduction in sensitivity corresponds to an overall increase in experimental times by a factor 144, necessitating sensitivity enhancement by ^{1}H detection or DNP for ^{195}Pt SSNMR experiments on **1@SiO₂**.

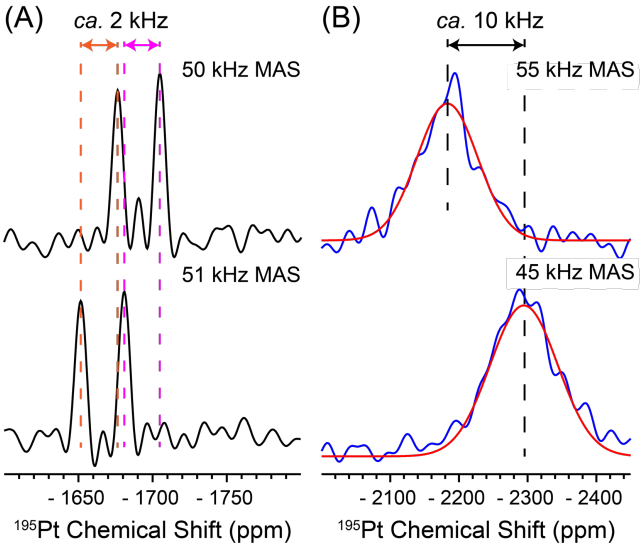

Figure 3. ^{195}Pt SSNMR spectra extracted from rotor-synchronized 2D $^{1}H\{^{195}Pt\}$ TONE D-HMQC-4 spectra of (A) **1** and (B) **1@SiO₂**. B_0 = 9.4 T and experimental MAS frequencies are indicated.

Constant-time $^{1}H\{^{195}Pt\}$ D-HMQC with rotor-asynchronous sampling of the indirect dimension can be used to obtain the full sideband manifold of the ^{195}Pt CSA pattern, which can be used to determine both the isotropic chemical shift and CSA parameters.[46] However, the sensitivity of $^{1}H\{^{195}Pt\}$ D-HMQC spectra obtained with rotor-synchronized t_1-intervals will be approximately 10-20 times higher because of spectral aliasing of all intensity into a single sideband. The isotropic ^{195}Pt chemical shift can be precisely determined by obtaining rotor-synchronized 2D $^{1}H\{^{195}Pt\}$ D-HMQC spectra with different MAS frequencies.[47-48] Figure 3 shows the ^{195}Pt NMR spectra

extracted from rotor-synchronized 2D $^{1}H\{^{195}Pt\}$ TONE D-HMQC-4 spectra of **1** and **1@SiO$_2$**; notably, the complete 2D spectra were obtained within reasonable experimental times of *ca.* 13 minutes and 10.5 hours for **1** and **1@SiO$_2$**, respectively (Figure S4). The value of the TONE D-HMQC-4 is evident in comparison to conventional D-HMQC spectra that show significant t_1-noise and inhibit spectral interpretation (Figure S4).

There are two signals in the ^{195}Pt SSNMR spectra of **1** (Figure 3A), consistent with the presence of two molecules in the asymmetric unit of its crystal structure.[49] The difference in isotropic shifts between the two sites likely arises from slight differences in local bond angles such as Si-O-Pt (*ca.* 136° and 144°) and O-Pt-C (161° and 166°, respectively).[49] Upon varying the MAS frequency from 50 to 51 kHz, it is observed that both signals shift positively by 2 kHz. This must mean that the observed peaks correspond to the second spinning sidebands from the isotropic shift in the positive direction. Since spinning sidebands appear exactly at integer multiples of the MAS frequency, the positions of other sidebands or center band are easily calculated.[48] For **1** the isotropic shifts of the two ^{195}Pt NMR signals are precisely determined to be –2867 and –2838 ppm. The observed values are consistent with the previously reported ^{195}Pt solution NMR shift of –2857 ppm.[49] Figure 3B shows ^{195}Pt SSNMR spectra of **1@SiO$_2$** extracted from 2D $^{1}H\{^{195}Pt\}$ TONE D-HMQC spectra obtained at 55 and 45 kHz MAS frequencies. The ^{195}Pt SSNMR spectra of **1@SiO$_2$** show broad peaks that can be fit to Gaussian functions, indicating there is a distribution of ^{195}Pt isotropic chemical shifts. The distribution in isotropic shifts is expected and likely reflects the inherently disordered nature of the silica surface, which will result in a range of bond lengths and angles.[11, 14-15, 78] As the ^{195}Pt signal of **1@SiO$_2$** moved by 10 kHz frequency upon varying the MAS frequency from 55 to 45 kHz, the observed signal must correspond to the first sideband and the center of the Gaussian isotropic shift distribution is determined to be –2819 ppm.

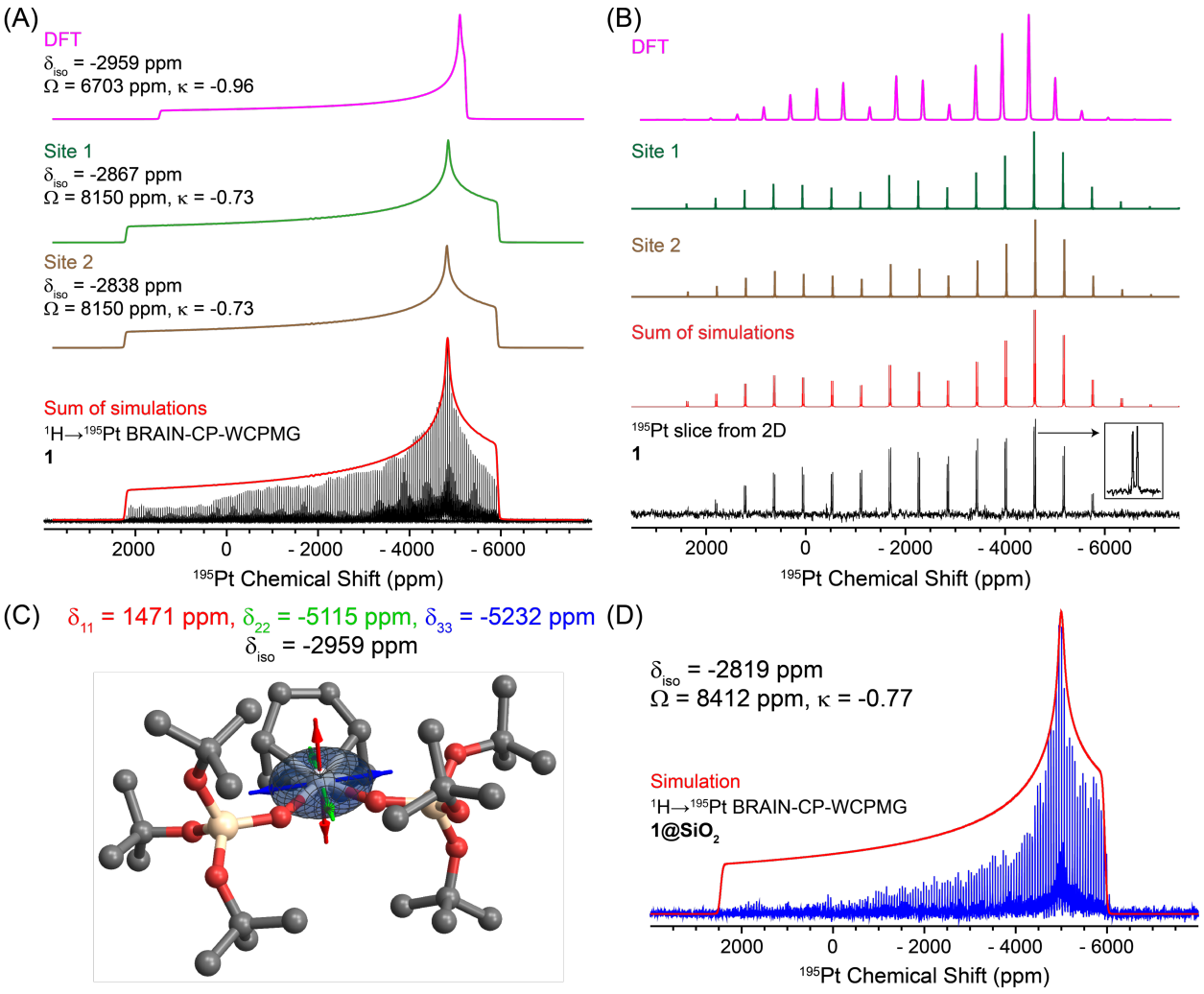

Figure 4. (A, black trace) Conventional $^{1}H \rightarrow ^{195}Pt$ BRAIN-CP-WCPMG spectrum of **1** at B_0 = 11.7 T and 298 K. (B, black trace) ^{195}Pt MAS SSNMR spectra extracted from 2D $^{1}H\{^{195}Pt\}$ TONE D-HMQC-4 spectrum; inset shows the resolution of two signals. Analytical simulations (green and brown traces) corresponding to the two ^{195}Pt sites in **1** and (pink trace) a spectrum simulated with CSA parameters from the DFT calculation. (C) DFT optimized structure of **1** showing the principal components of the ^{195}Pt CS tensor; hydrogens are omitted for clarity. (D) DNP enhanced $^{1}H \rightarrow ^{195}Pt$ BRAIN-CP-WCPMG spectrum of **1@SiO$_2$** at B_0 = 9.4 T and 105 K. A single-site simulation was performed with Gaussian broadening to model the distribution in isotropic shifts (red trace). Fitted CS tensor parameters are indicated.

Figure 4A shows a $^{1}H \rightarrow ^{195}Pt$ static BRAIN-CP-WCPMG spectrum of **1** (black trace) that was obtained with the VOCS (variable offset cumulative spectrum) acquisition method[56, 79] during a total experimental time of *ca.* 3 days (pulse sequence is shown in Figure S5). Using the ^{195}Pt isotropic shifts of **1** from the fast MAS measurements and the observed span (Ω) of the static

spectrum (*ca.* 8150 ppm), the skew of the CS tensor (κ) was determined to be –0.73 for both ^{195}Pt sites in **1** (green and brown traces, Figure 4A). The sum of the two simulations is shown to fit the experimental spectrum accurately (red trace, Figure 4A). The Ω and κ values derived from this fitting procedure were further confirmed by comparing a simulation of the sideband manifold at 50 kHz with the ^{195}Pt slice obtained with TONE D-HMQC-4 at 50 kHz MAS (Figure 4B, Figure S6). Indeed, fast MAS enables the resolution of the two sets of sidebands and confirms that the two ^{195}Pt sites display the same CSA parameters (Ω = 8150 ppm and κ = –0.73). Figure 4C shows a DFT optimized structure of **1** and the predicted ^{195}Pt CS tensor; simulations based on the DFT parameters (δ_{iso} = –2959 ppm, Ω = 6703 ppm and κ = –0.96) agree reasonably with the experimental ^{195}Pt NMR spectra (pink traces, Figure 4A and 4B), considering the large CSA, the high sensitivity of ^{195}Pt chemical shift to the ligand environment,[27,29] and the challenges associated with accurately calculating chemical shifts for heavy nuclei.

The low concentration of surface Pt sites necessitated DNP-SENS to obtain static ^{195}Pt SSNMR spectra of **1@SiO$_2$** (Figure 4D). A favorable ^{1}H solvent DNP enhancement of 110 was measured under static conditions. The DNP enhancement for **1@SiO$_2$** was also measured under MAS by examining the ^{13}C NMR signals of the ligands and ^{29}Si NMR signals of the silica surface (Figure S7 and S8). Comparison of the ^{13}C CPMAS spectra shows that the ligand structure is intact upon grafting (Figure S7). A ^{1}H→^{29}Si CP enhancement of 80 was observed and Q_{3M} site of the OSi(O*t*Bu)$_3$ ligand is observed at -87 ppm, in good agreement with the previous reported solution NMR shift of the precursor at -88 ppm (Figure S8).[49] Despite the DNP signal enhancements, the ^{1}H→^{195}Pt static BRAIN-CP-WCPMG spectrum of **1@SiO$_2$** was obtained in 5 days of acquisition time. Due to the low sensitivity, constant-time TONE D-HMQC-4 experiments needed to observe the full ^{195}Pt sideband manifold were not feasible, demonstrating the value of DNP. Extracting the

mean isotropic chemical shift of the Gaussian distribution of ^{195}Pt isotropic shifts measured for **1@SiO$_2$** (–2819 ppm, *vide supra*) and using the width of the distribution as a starting parameter, fitting of the static DNP-SENS spectrum with 8 kHz of Gaussian broadening gave Ω and κ values of 8412 ppm and –0.77, respectively. The similarity of the fitted CSA parameters of **1@SiO$_2$** to those of **1** is consistent with a similar Pt chemical environment and with the proposed structure of the surface-bound Pt(II) complex (Figure 1B).

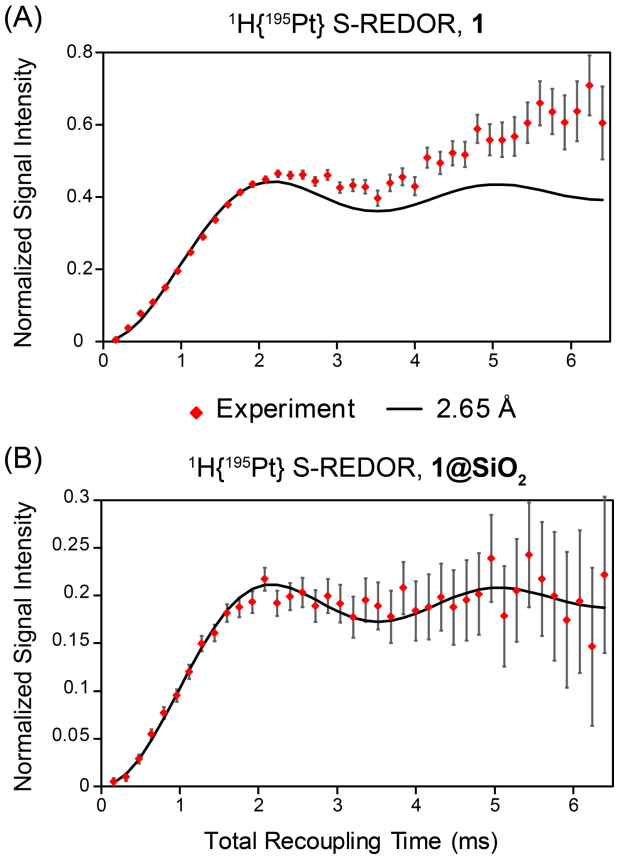

Figure 5. ^{1}H{^{195}Pt} S-REDOR measurements on samples (A) **1** and (B) **1@SiO$_2$**. The dipolar dephasing curves were extracted from a ^{1}H chemical shift of (A) 5.7 ppm and (B) 5.5 ppm that corresponds to the alkene hydrogen of the COD ligand. Experimental data points [1-(S/S_0)-ϕ)] are plotted as red diamonds and SIMPSON numerical simulations [f×(1- (S/S_0))] as black lines. ϕ is equal to 0.08 and 0.05, and f is equal to 0.46 and 0.22, in (A) and (B), respectively. Experiments were performed at 50 kHz MAS and B_0 = 9.4 T.

Finally, ^{1}H{^{195}Pt} S-REDOR[54] experiments with $SR4_1^2$ heteronuclear dipolar recoupling[50] were used to measure the ^{1}H-^{195}Pt dipolar coupling constants and internuclear distances between

the vinyl protons of the COD ligand and the Pt center in both **1** and **1@SiO$_2$** (Figure 5). The S-REDOR curve corresponding to the COD alkene proton resonance at 5.7 ppm for **1** was fit to a dipolar coupling of 1.4 kHz and a distance of 2.65 Å by minimizing the root mean square deviation (RMSD) between the fitted and experimental data points (Figure 5A and Figure S9). Note that only experimental data up to 2 ms of recoupling were considered as additional dephasing of the ^{1}H signal is observed at longer recoupling durations due to long-distance Pt-H contacts with Pt atoms in the adjacent molecules in the crystal lattice. However, the experimental S-REDOR curve for the COD alkene ^{1}H in **1@SiO$_2$** can be fit precisely to a 2.65 Å with data points up to 6.4 ms of recoupling included in the RMSD analysis (Figure 5B and Figure S9). The observation that the S-REDOR curve for **1@SiO$_2$** does not show increased dephasing at longer recoupling times is consistent with isolation of Pt sites on the silica surface; there should be a low probability of a second ^{195}Pt spin being found within a 5 Å radius from the vinyl hydrogen atom due to the 0.6 Pt site/nm^2 surface coverage. The measured Pt-H distances are in good agreement with the average Pt-alkene H distance of 2.63 Å predicted for the DFT optimized structure of **1**. Periodic plane-wave DFT optimization of the hydrogen atom positions using the single-crystal structure as the input also provides a similar average Pt-H distance of 2.62 Å. Note that the DFT calculations were performed under standard conditions that assume 0 K temperature and hydrogen atom positions may change with temperature.[80] In both **1** and **1@SiO$_2$**, slower dephasing is also observed for the methyl groups at 1.2-1.4 ppm due to longer Pt-H distances (5-7 Å) and correspondingly weaker Pt-H dipolar couplings (Figure S10). At 6.4 ms of recoupling, the ^{1}H{^{195}Pt} S-REDOR experiments shows higher signal dephasing for the methyl ^{1}H NMR signal of **1** (dephasing of 0.14) in comparison to the methyl signal of **1@SiO$_2$** (0.04). The higher dephasing for the methyl groups of **1** is likely caused by the presence of adjacent Pt spins in the crystalline lattice and the lack of a

close Pt-H contact that dominates the dephasing. Different methyl group dynamics in **1** and **1@SiO$_2$** may also affect dephasing. Nevertheless, the observed dipolar dephasing for methyl groups confirms that the siloxide ligands are indeed retained in the grafted compound. In summary, the ^{1}H{^{195}Pt} S-REDOR experiments provide further confirmation that the proposed model of the grafted complex in Figure 1B is the correct surface structure.

Conclusions

Fast MAS, proton-detected SSNMR was used to determine the isotropic shifts of an isolated ^{195}Pt surface complex with 3.7 wt.% Pt loading and of its molecular precursor. ^{195}Pt chemical shift anisotropies were measured with BRAIN-CP-WCPMG experiments, with signal enhancements provided by DNP for the surface complex. The isotropic shifts obtained by fast MAS experiments were crucial to constrain the fits of ^{195}Pt static CSA patterns. The observation of a single Pt site in **1@SiO$_2$** with CSA parameters similar to the molecular precursor **1** confirms that the Pt site is well-defined in **1@SiO$_2$**, where the distribution of isotropic shifts is likely due to small variations in local bond angles associated with the presence of different local environments arising because of the amorphous surface structure of silica. These conclusions are validated by ^{1}H-^{195}Pt inter-nuclear distance measurements, which indicate that the local geometry of the Pt metal center is unchanged in the precursor and on the silica surface. Considering the signal-to-noise ratios and required experiment times, the methods proposed here should be applicable to Pt SAC with a Pt loading of ca. 1 wt.% (see additional discussion in SI). Furthermore, the future combination of DNP-SENS with fast MAS and proton detection[81-83] could yield further gains in sensitivity that would aid in the characterization of low Pt loading catalysts.

Acknowledgements

Fast MAS solid-state NMR spectroscopy experiments and data analysis (AV and AJR) were supported by the National Science Foundation under Grant No. 1709972 to AJR. AV and AJR acknowledge additional support from Donors of the American Chemical Society Petroleum Research Fund (58627-DNI6). AJR acknowledges additional support from the Alfred P. Sloan Foundation through a Sloan research fellowship. LR and CPG thank the SNF (SNSF fond number: 200021_169134) and the Scholarship Fund of the Swiss Chemical Industry (SSCI) for funding, respectively. Financial support from ANR-17-CE29-0006-01 is also gratefully acknowledged.

Supporting Information

Pulse sequence diagrams, pulse programs, additional 1D and 2D NMR spectra, and fits of the S-REDOR curves. This material is available free of charge via the Internet at http://pubs.acs.org. Raw NMR data and pulse sequences have been deposited at http://10.5281/zenodo.4062776

References

1. Bowker, M. *The Basis and Applications of Heterogeneous Catalysis*, 1st Edition; Oxford University Press: Oxford, 1998.
2. Coperet, C.; Comas-Vives, A.; Conley, M. P.; Estes, D. P.; Fedorov, A.; Mougel, V.; Nagae, H.; Nunez-Zarur, F.; Zhizhko, P. A. Surface Organometallic and Coordination Chemistry toward Single-Site Heterogeneous Catalysts: Strategies, Methods, Structures, and Activities. *Chem. Rev.* **2016,** *116* (2), 323-421.
3. Wang, A. Q.; Li, J.; Zhang, T. Heterogeneous Single-Atom Catalysis. *Nat. Rev. Chem.* **2018,** *2* (6), 65-81.
4. Wegener, S. L.; Marks, T. J.; Stair, P. C. Design Strategies for the Molecular Level Synthesis of Supported Catalysts. *Acc. Chem. Res.* **2012,** *45* (2), 206-214.
5. Pelletier, J. D. A.; Basset, J. M. Catalysis by Design: Well-Defined Single-Site Heterogeneous Catalysts. *Acc. Chem. Res.* **2016,** *49* (4), 664-677.
6. Laurent, P.; Veyre, L.; Thieuleux, C.; Donet, S.; Coperet, C. From Well-Defined Pt(II) Surface Species to the Controlled Growth of Silica Supported Pt Nanoparticles. *Dalton Trans.* **2013,** *42* (1), 238-248.
7. Searles, K.; Chan, K. W.; Burak, J. A. M.; Zemlyanov, D.; Safonova, O.; Coperet, C. Highly Productive Propane Dehydrogenation Catalyst Using Silica-Supported Ga-Pt Nanoparticles Generated from Single-Sites. *J. Am. Chem. Soc.* **2018,** *140* (37), 11674-11679.
8. Coperet, C. Single-Sites and Nanoparticles at Tailored Interfaces Prepared via Surface Organometallic Chemistry from Thermolytic Molecular Precursors. *Acc. Chem. Res.* **2019,** *52* (6), 1697-1708.
9. Rochlitz, L.; Searles, K.; Alfke, J.; Zemlyanov, D.; Safonova, O. V.; Coperet, C. Silica-Supported, Narrowly Distributed, Subnanometric Pt-Zn Particles from Single Sites with High Propane Dehydrogenation Performance. *Chem. Sci.* **2020,** *11* (6), 1549-1555.
10. Zhang, W. P.; Xu, S. T.; Han, X. W.; Bao, X. H. In Situ Solid-State NMR for Heterogeneous Catalysis: A Joint Experimental and Theoretical Approach. *Chem. Soc. Rev.* **2012,** *41* (1), 192-210.
11. D'Elia, V.; Dong, H. L.; Rossini, A. J.; Widdifield, C. M.; Vummaleti, S. V. C.; Minenkov, Y.; Poater, A.; Abou-Hamad, E.; Pelletier, J. D. A.; Cavallo, L.; Emsley, L.; Basset, J. M. Cooperative Effect of Monopodal Silica-Supported Niobium Complex Pairs Enhancing Catalytic Cyclic Carbonate Production. *J. Am. Chem. Soc.* **2015,** *137* (24), 7728-7739.

12. Kobayashi, T.; Perras, F. A.; Slowing, I. I.; Sadow, A. D.; Pruski, M. Dynamic Nuclear Polarization Solid-State NMR in Heterogeneous Catalysis Research. *ACS Catal.* **2015,** *5* (12), 7055-7062.
13. Coperet, C.; Liao, W. C.; Gordon, C. P.; Ong, T. C. Active Sites in Supported Single-Site Catalysts: An NMR Perspective. *J. Am. Chem. Soc.* **2017,** *139* (31), 10588-10596.
14. Vancompernolle, T.; Trivelli, X.; Delevoye, L.; Pourpoint, F.; Gauvin, R. M. On the use of Solid-State ^{45}Sc NMR for Structural Investigations of Molecular and Silica-Supported Scandium Amide Catalysts. *Dalton Trans.* **2017,** *46* (39), 13176-13179.
15. Grekov, D.; Vancompernolle, T.; Taoufik, M.; Delevoye, L.; Gauvin, R. M. Solid-State NMR of Quadrupolar Nuclei for Investigations into Supported Organometallic Catalysts: Scope and Frontiers. *Chem. Soc. Rev.* **2018,** *47* (8), 2572-2590.
16. Culver, D. B.; Venkatesh, A.; Huynh, H.; Rossini, A. J.; Conley, M. P. $Al(OR^F)_3$ ($R^F = C(CF_3)_3$) Activated Silica: A Well-Defined Weakly Coordinating Surface Anion. *Chem. Sci.* **2020,** *11* (6), 1510-1517.
17. Mance, D.; Comas-Vives, A.; Coperet, C. Proton-Detected Multidimensional Solid-State NMR Enables Precise Characterization of Vanadium Surface Species at Natural Abundance. *J. Phys. Chem. Lett.* **2019,** *10* (24), 7898-7904.
18. Vajda, S.; Pellin, M. J.; Greeley, J. P.; Marshall, C. L.; Curtiss, L. A.; Ballentine, G. A.; Elam, J. W.; Catillon-Mucherie, S.; Redfern, P. C.; Mehmood, F.; Zapol, P. Subnanometre Platinum Clusters as Highly Active and Selective Catalysts for the Oxidative Dehydrogenation of Propane. *Nat. Mater.* **2009,** *8* (3), 213-216.
19. Qiao, B. T.; Wang, A. Q.; Yang, X. F.; Allard, L. F.; Jiang, Z.; Cui, Y. T.; Liu, J. Y.; Li, J.; Zhang, T. Single-atom catalysis of CO oxidation using Pt-1/FeOx. *Nat. Chem.* **2011,** *3* (8), 634-641.
20. Fu, Q.; Saltsburg, H.; Flytzani-Stephanopoulos, M. Active Nonmetallic Au and Pt Species on Ceria-based Water-Gas Shift Catalysts. *Science* **2003,** *301* (5635), 935-938.
21. Cui, X. J.; Li, W.; Ryabchuk, P.; Junge, K.; Beller, M. Bridging Homogeneous and Heterogeneous catalysis by Heterogeneous Single-Metal-Site Catalysts. *Nat. Catal.* **2018,** *1* (6), 385-397.
22. Liu, Q.; Zhang, Z. L. Platinum Single-Atom Catalysts: A Comparative Review Towards Effective Characterization. *Catal. Sci. Technol.* **2019,** *9* (18), 4821-4834.
23. Hannagan, R. T.; Giannakakis, G.; Flytzani-Stephanopoulos, M.; Sykes, E. C. H. Single-Atom Alloy Catalysis. *Chem Rev* **2020**, DOI: 10.1021/acs.chemrev.0c00078.
24. Yang, X. F.; Wang, A. Q.; Qiao, B. T.; Li, J.; Liu, J. Y.; Zhang, T. Single-Atom Catalysts: A New Frontier in Heterogeneous Catalysis. *Acc. Chem. Res.* **2013,** *46* (8), 1740-1748.
25. Gao, C.; Low, J.; Long, R.; Kong, T.; Zhu, J.; Xiong, Y. Heterogeneous Single-Atom Photocatalysts: Fundamentals and Applications. *Chem. Rev.* **2020**, DOI: 10.1021/acs.chemrev.9b00840.
26. Sparks, S. W.; Ellis, P. D. ^{195}Pt Shielding Tensors in Potassium Hexachloroplatinate(IV) and Potassium Tetrachloroplatinate(II). *J. Am. Chem. Soc.* **1986,** *108* (12), 3215-3218.
27. Austin, E. J. W.; Barrie, P. J.; Clark, R. J. H. Solid-State ^{195}Pt NMR-Studies of the Complexes $Pt(En)Cl_x$ (En = 1,2-Diaminoethane x = 2,3 or 4). *J. Chem. Soc., Chem. Commun.* **1993,** (18), 1404-1405.
28. Sterzel, M.; Autschbach, J. Toward an Accurate Determination of ^{195}Pt Chemical Shifts by Density Functional Computations: The Importance of Unspecific Solvent Effects and the Dependence of Pt Magnetic Shielding Constants on Structural Parameters. *Inorg. Chem.* **2006,** *45* (8), 3316-3324.
29. Autschbach, J.; Zheng, S. H. Analyzing Pt Chemical Shifts Calculated from Relativistic Density Functional Theory Using Localized Orbitals: The Role of Pt 5d Lone Pairs. *Magn. Reson. Chem.* **2008,** *46*, S45-S55.
30. Lucier, B. E. G.; Reidel, A. R.; Schurko, R. W. Multinuclear Solid-State NMR of Square-Planar Platinum Complexes - Cisplatin and Related Systems. *Can. J. Chem.* **2011,** *89* (7), 919-937.
31. Rees, G. J.; Orr, S. T.; Barrett, L. O.; Fisher, J. M.; Houghton, J.; Spikes, G. H.; Theobald, B. R. C.; Thompsett, D.; Smith, M. E.; Hanna, J. V. Characterisation of Platinum-Based Fuel Cell Catalyst Materials Using ^{195}Pt Wideline Solid State NMR. *Phys. Chem. Chem. Phys.* **2013,** *15* (40), 17195-17207.

32. Lucier, B. E. G.; Johnston, K. E.; Xu, W. Q.; Hanson, J. C.; Senanayake, S. D.; Yao, S. Y.; Bourassa, M. W.; Srebro, M.; Autschbach, J.; Schurko, R. W. Unravelling the Structure of Magnus' Pink Salt. *J. Am. Chem. Soc.* **2014,** *136* (4), 1333-1351.
33. Kobayashi, T.; Perras, F. A.; Goh, T. W.; Metz, T. L.; Huang, W. Y.; Pruski, M. DNP-Enhanced Ultrawideline Solid-State NMR Spectroscopy: Studies of Platinum in Metal-Organic Frameworks. *J. Phys. Chem. Lett.* **2016,** *7* (13), 2322-2327.
34. Soorholtz, M.; Jones, L. C.; Samuelis, D.; Weidenthaler, C.; White, R. J.; Titirici, M. M.; Cullen, D. A.; Zimmermann, T.; Antonietti, M.; Maier, J.; Palkovits, R.; Chmelka, B. F.; Schuth, F. Local Platinum Environments in a Solid Analogue of the Molecular Periana Catalyst. *ACS Catal.* **2016,** *6* (4), 2332-2340.
35. Perras, F. A.; Venkatesh, A.; Hanrahan, M. P.; Goh, T. W.; Huang, W.; Rossini, A. J.; Pruski, M. Indirect Detection of Infinite-Speed MAS Solid-State NMR Spectra. *J. Magn. Reson.* **2017,** *276*, 95-102.
36. Camacho-Bunquin, J.; Ferrandon, M.; Sohn, H.; Yang, D. L.; Liu, C.; Ignacio-de Leon, P. A.; Perras, F. A.; Pruski, M.; Stair, P. C.; Delferro, M. Chemoselective Hydrogenation with Supported Organoplatinum(IV) Catalyst on Zn(II)-Modified Silica. *J. Am. Chem. Soc.* **2018,** *140* (11), 3940-3951.
37. Semenov, V. A.; Samultsev, D. O.; Rusakova, I. L.; Krivdin, L. B. Computational Multinuclear NMR of Platinum Complexes: A Relativistic Four-Component Study. *J. Phys. Chem. A* **2019,** *123* (23), 4908-4920.
38. Harris, K. J.; Lupulescu, A.; Lucier, B. E. G.; Frydman, L.; Schurko, R. W. Broadband Adiabatic Inversion Pulses for Cross Polarization in Wideline Solid-State NMR Spectroscopy. *J. Magn. Reson.* **2012,** *224*, 38-47.
39. MacGregor, A. W.; O'Dell, L. A.; Schurko, R. W. New Methods for the Acquisition of Ultra-Wideline Solid-State NMR Spectra of Spin-1/2 Nuclides. *J. Magn. Reson.* **2011,** *208* (1), 103-113.
40. Rossini, A. J.; Zagdoun, A.; Lelli, M.; Lesage, A.; Copéret, C.; Emsley, L. Dynamic Nuclear Polarization Surface Enhanced NMR Spectroscopy. *Acc. Chem. Res.* **2013,** *46* (9), 1942-1951.
41. Berruyer, P.; Lelli, M.; Conley, M. P.; Silverio, D. L.; Widdifield, C. M.; Siddiqi, G.; Gajan, D.; Lesage, A.; Coperet, C.; Emsley, L. Three-Dimensional Structure Determination of Surface Sites. *J. Am. Chem. Soc.* **2017,** *139* (2), 849-855.
42. Blanc, F. Investigation of Catalytic Surfaces with Surface-Enhanced Solid-State NMR Spectroscopy. *Nanotechnology in Catalysis* **2017**, 1003-1028.
43. Liao, W. C.; Ghaffari, B.; Gordon, C. P.; Xu, J.; Coperet, C. Dynamic Nuclear Polarization Surface Enhanced NMR spectroscopy (DNP SENS): Principles, Protocols, and Practice. *Curr. Opin. Colloid Interface Sci.* **2018,** *33*, 63-71.
44. Ishii, Y.; Yesinowski, J. P.; Tycko, R. Sensitivity Enhancement in Solid-State ^{13}C NMR of Synthetic Polymers and Biopolymers by ^{1}H NMR Detection with High-Speed Magic Angle Spinning. *J. Am. Chem. Soc.* **2001,** *123* (12), 2921-2922.
45. Poppler, A. C.; Demers, J. P.; Malon, M.; Singh, A. P.; Roesky, H. W.; Nishiyama, Y.; Lange, A. Ultrafast Magic-Angle Spinning: Benefits for the Acquisition of Ultrawide-Line NMR Spectra of Heavy Spin-1/2 Nuclei. *Chemphyschem* **2016,** *17* (6), 812-816.
46. Rossini, A. J.; Hanrahan, M. P.; Thuo, M. Rapid Acquisition of Wideline MAS Solid-State NMR Spectra with Fast MAS, Proton Detection, and Dipolar HMQC Pulse Sequences. *Phys. Chem. Chem. Phys.* **2016,** *18* (36), 25284-25295.
47. Li, Y. X.; Trebosc, J.; Hu, B. W.; Shen, M.; Amoureux, J. P.; Lafon, O. Indirect detection of Broad Spectra in Solid-State NMR Using Interleaved DANTE Trains. *J. Magn. Reson.* **2018,** *294*, 101-114.
48. Paluch, P.; Rankin, A. G. M.; Trebosc, J.; Lafon, O.; Amoureux, J. P. Analysis of HMQC Experiments Applied to a Spin 1/2 Nucleus Subject to Very Large CSA. *Solid State Nucl. Magn. Reson.* **2019,** *100*, 11-25.
49. Ruddy, D. A.; Jarupatrakorn, J.; Rioux, R. M.; Miller, J. T.; McMurdo, M. J.; Mcbee, J. L.; Tupper, K. A.; Tilley, T. D. Site-Isolated Pt-SBA15 Materials from Tris(tert-butoxy)siloxy Complexes of Pt(II) and Pt(IV). *Chem. Mater.* **2008,** *20* (20), 6517-6527.

50. Brinkmann, A.; Kentgens, A. P. M. Proton-Selective ^{17}O-^{1}H Distance Measurements in Fast Magic Angle Spinning Solid-State NMR Spectroscopy for the Determination of Hydrogen Bond Lengths. *J. Am. Chem. Soc.* **2006,** *128* (46), 14758-14759.
51. Marion, D.; Ikura, M.; Tschudin, R.; Bax, A. Rapid Recording of 2D NMR-Spectra without Phase Cycling - Application to the Study of Hydrogen-Exchange in Proteins. *J. Magn. Reson.* **1989,** *85* (2), 393-399.
52. van Meerten, S. G. J.; Franssen, W. M. J.; Kentgens, A. P. M. ssNake: A cross-Platform Open-Source NMR Data Processing and Fitting Application. *J. Magn. Reson.* **2019,** *301*, 56-66.
53. Venkatesh, A.; Hung, I.; Boteju, K. C.; Sadow, A. D.; Gor'kov, P. L.; Gan, Z.; Rossini, A. J. Suppressing ^{1}H Spin Diffusion in Fast MAS Proton Detected Heteronuclear Correlation Solid-State NMR Experiments. *Solid State Nucl. Magn. Reson.* **2020,** *105*, 101636.
54. Chen, L.; Wang, Q. A.; Hu, B. W.; Lafon, O.; Trebosc, J.; Deng, F.; Amoureux, J. P. Measurement of Hetero-Nuclear Distances Using a Symmetry-Based Pulse Sequence in Solid-State NMR. *Phys. Chem. Chem. Phys.* **2010,** *12* (32), 9395-9405.
55. Duong, N. T.; Rossi, F.; Makrinich, M.; Goldbourt, A.; Chierotti, M. R.; Gobetto, R.; Nishiyama, Y. Accurate ^{1}H-^{14}N Distance Measurements by Phase-Modulated RESPDOR at Ultra-Fast MAS. *J. Magn. Reson.* **2019,** *308*, 106559.
56. Massiot, D.; Farnan, I.; Gautier, N.; Trumeau, D.; Trokiner, A.; Coutures, J. P. ^{71}Ga and ^{69}Ga Nuclear-Magnetic-Resonance Study of Beta-Ga_2O_3 - Resolution of 4-Fold and 6-Fold Coordinated Ga Sites in Static Conditions. *Solid State Nucl. Magn. Reson.* **1995,** *4* (4), 241-248.
57. Rosay, M.; Tometich, L.; Pawsey, S.; Bader, R.; Schauwecker, R.; Blank, M.; Borchard, P. M.; Cauffman, S. R.; Felch, K. L.; Weber, R. T.; Temkin, R. J.; Griffin, R. G.; Maas, W. E. Solid-state dynamic nuclear polarization at 263 GHz: spectrometer design and experimental results. *Phys. Chem. Chem. Phys.* **2010,** *12* (22), 5850-5860.
58. Zagdoun, A.; Casano, G.; Ouari, O.; Schwarzwälder, M.; Rossini, A. J.; Aussenac, F.; M., Y.; G., J.; Copéret, C.; Lesage, A.; Tordo, P.; Emsley, L. Large Molecular Weight Nitroxide Biradicals Providing Efficient Dynamic Nuclear Polarization at Temperatures up to 200 K. *J. Am. Chem. Soc.* **2013,** *135* (34), 12790-12797.
59. Massiot, D.; Fayon, F.; Capron, M.; King, I.; Le Calve, S.; Alonso, B.; Durand, J. O.; Bujoli, B.; Gan, Z. H.; Hoatson, G. Modelling one- and two-dimensional solid-state NMR spectra. *Magn. Reson. Chem.* **2002,** *40* (1), 70-76.
60. Yarava, J. R.; Chaudhari, S. R.; Rossini, A. J.; Lesage, A.; Emsley, L. Solvent suppression in DNP enhanced solid state NMR. *J. Magn. Reson.* **2017,** *277*, 149-153.
61. Frisch, M. J.; Trucks, G. W.; Schlegel, H. B.; Scuseria, G. E.; Robb, M. A.; Cheeseman, J. R.; Scalmani, G.; Barone, V.; Mennucci, B.; Petersson, G. A.; Nakatsuji, H.; Caricato, M.; Li, X.; Hratchian, H. P.; Izmaylov, A. F.; Bloino, J.; Zheng, G.; Sonnenberg, J. L.; Hada, M.; Ehara, M.; Toyota, K.; Fukuda, R.; Hasegawa, J.; Ishida, M.; Nakajima, T.; Honda, Y.; Kitao, O.; Nakai, H.; Vreven, T.; Montgomery, J. A.; Peralta, J. J. E.; Ogliaro, F.; Bearpark, M.; Heyd, J. J.; Brothers, E.; Kudin, K. N.; Staroverov, V. N.; Kobayashi, R.; Normand, J.; Raghavachari, K.; Rendell, A.; Burant, J. C.; Iyengar, S. S.; Tomasi, J.; Cossi, M.; Rega, N.; Millam, J. M.; Klene, M.; Knox, J. E.; Cross, J. B.; Bakken, V.; Adamo, C.; Jaramillo, J.; Gomperts, R.; Stratmann, R. E.; Yazyev, O.; Austin, A. J.; Cammi, R.; Pomelli, C.; Ochterski, J. W.; Martin, R. L.; Morokuma, K.; Zakrzewski, V. G.; Voth, G. A.; Salvador, P.; Dannenberg, J. J.; Dapprich, S.; Daniels, A. D.; Farkas, Ö.; Foresman, J. B.; Ortiz, J. V.; Cioslowski, J.; Fox, D. J. *Gaussian 09 Version D.01*, Gaussian Inc.: Wallingford, CT, 2009.
62. Adamo, C.; Barone, V. Toward Reliable Density Functional Methods Without Adjustable Parameters: The PBE0 model. *J. Chem. Phys.* **1999,** *110* (13), 6158-6170.
63. Figgen, D.; Peterson, K. A.; Dolg, M.; Stoll, H. Energy-Consistent Pseudopotentials and Correlation Consistent Basis Sets for the 5d Elements Hf-Pt. *J. Chem. Phys.* **2009,** *130* (16), 164108.
64. Dunning, T. H. Gaussian-Basis Sets for Use in Correlated Molecular Calculations .1. The Atoms Boron through Neon and Hydrogen. *J. Chem. Phys.* **1989,** *90* (2), 1007-1023.

65. te Velde, G.; Bickelhaupt, F. M.; Baerends, E. J.; Guerra, C. F.; Van Gisbergen, S. J. A.; Snijders, J. G.; Ziegler, T. Chemistry with ADF. *J. Comput. Chem.* **2001,** *22* (9), 931-967.
66. vanLenthe, E.; vanLeeuwen, R.; Baerends, E. J.; Snijders, J. G. Relativistic Regular Two-Component Hamiltonians. *Int. J. Quantum Chem.* **1996,** *57* (3), 281-293.
67. Zurek, E.; Pickard, C. J.; Autschbach, J. Density Functional Study of the ^{13}C NMR Chemical Shifts in Single-Walled Carbon Nanotubes with Stone-Wales Defects. *J. Phys. Chem. C* **2008,** *112* (31), 11744-11750.
68. Clark, S. J.; Segall, M. D.; Pickard, C. J.; Hasnip, P. J.; Probert, M. J.; Refson, K.; Payne, M. C. First Principles Methods using CASTEP. *Z. Kristallogr.* **2005,** *220* (5-6), 567-570.
69. Perdew, J. P.; Burke, K.; Ernzerhof, M. Generalized Gradient Approximation Made Simple. *Phys. Rev. Lett.* **1996,** *77* (18), 3865-3868.
70. Tkatchenko, A.; Scheffler, M. Accurate Molecular Van Der Waals Interactions from Ground-State Electron Density and Free-Atom Reference Data. *Phys. Rev. Lett.* **2009,** *102* (7), 073005.
71. Yates, J. R.; Pickard, C. J.; Mauri, F. Calculation of NMR Chemical Shifts for Extended Systems using Ultrasoft Pseudopotentials. *Phys. Rev. B* **2007,** *76* (2), 024401.
72. Pickard, C. J.; Mauri, F. All-Electron Magnetic Response with Pseudopotentials: NMR Chemical Shifts. *Phys. Rev. B* **2001,** *63* (24), 245101.
73. Green, T. F. G.; Yates, J. R. Relativistic Nuclear Ragnetic Resonance J-Coupling with Ultrasoft Pseudopotentials and the Zeroth-Order Regular Approximation. *J. Chem. Phys.* **2014,** *140* (23), 234106.
74. Venkatesh, A.; Luan, X.; Perras, F. A.; Hung, I.; Huang, W.; Rossini, A. J. t_1-Noise Eliminated Dipolar Heteronuclear Multiple-Quantum Coherence Solid-State NMR Spectroscopy. *Phys. Chem. Chem. Phys.* **2020,** *22*, 20815-20828.
75. Kervern, G.; Pintacuda, G.; Emsley, L. Fast Adiabatic Pulses for Solid-State NMR of Paramagnetic Systems. *Chem. Phys. Lett.* **2007,** *435* (1-3), 157-162.
76. Sanders, K. J.; Pell, A. J.; Wegner, S.; Grey, C. P.; Pintacuda, G. Broadband MAS NMR Spectroscopy in the Low-Power Limit. *Chem. Phys. Lett.* **2018,** *697*, 29-37.
77. Trebosc, J.; Wiench, J. W.; Huh, S.; Lin, V. S. Y.; Pruski, M. Solid-State NMR Study of MCM-41-type Mesoporous Silica Nanoparticles. *J. Am. Chem. Soc.* **2005,** *127* (9), 3057-3068.
78. Delley, M. F.; Lapadula, G.; Nunez-Zarur, F.; Comas-Vives, A.; Kalendra, V.; Jeschke, G.; Baabe, D.; Walter, M. D.; Rossini, A. J.; Lesage, A.; Emsley, L.; Maury, O.; Coperet, C. Local Structures and Heterogeneity of Silica-Supported M(III) Sites Evidenced by EPR, IR, NMR, and Luminescence Spectroscopies. *J. Am. Chem. Soc.* **2017,** *139* (26), 8855-8867.
79. Schurko, R. W. Ultra-Wideline Solid-State NMR Spectroscopy. *Acc. Chem. Res.* **2013,** *46* (9), 1985-1995.
80. Martins, D. M. S.; Middlemiss, D. S.; Pulham, C. R.; Wilson, C. C.; Weller, M. T.; Henry, P. F.; Shankland, N.; Shankland, K.; Marshall, W. G.; Ibberson, R. M.; Knight, K.; Moggach, S.; Brunelli, M.; Morrison, C. A. Temperature- and Pressure-induced Proton Transfer in the 1:1 Adduct Formed between Squaric Acid and 4,4 '-Bipyridine. *J. Am. Chem. Soc.* **2009,** *131* (11), 3884-3893.
81. Wisser, D.; Karthikeyan, G.; Lund, A.; Casano, G.; Karoui, H.; Yulikov, M.; Menzildjian, G.; Pinon, A. C.; Purea, A.; Engelke, F.; Chaudhari, S. R.; Kubicki, D.; Rossini, A. J.; Moroz, I. B.; Gajan, D.; Coperet, C.; Jeschke, G.; Lelli, M.; Emsley, L.; Lesage, A.; Ouari, O. BDPA-Nitroxide Biradicals Tailored for Efficient Dynamic Nuclear Polarization Enhanced Solid-State NMR at Magnetic Fields up to 21.1 T. *J. Am. Chem. Soc.* **2018,** *140* (41), 13340-13349.
82. Wang, Z.; Hanrahan, M. P.; Kobayashi, T.; Perras, F. A.; Chen, Y.; Engelke, F.; Reiter, C.; Purea, A.; Rossini, A. J.; Pruski, M. Combining Fast Magic Angle Spinning Dynamic Nuclear Polarization with Indirect Detection to Further Enhance the Sensitivity of Solid-State NMR Spectroscopy. *Solid State Nucl. Magn. Reson.* **2020,** *109*, 101685.
83. Berruyer, P.; Björgvinsdóttir, S.; Bertarello, A.; Stevanato, G.; Rao, Y.; Karthikeyan, G.; Casano, G.; Ouari, O.; Lelli, M.; Reiter, C.; Engelke, F.; Emsley, L. Dynamic Nuclear Polarization Enhancement of 200 at 21.15 T Enabled by 65 kHz Magic Angle Spinning. *J. Phys. Chem. Lett.* **2020,** *11*, 8386-8391.

TOC graphic